The effects of supramolecular assembly on exciton decay rates in organic semiconductors

Clément Daniel, François Makereel, and Laura M. Herz[a)]
Cavendish Laboratory, University of Cambridge, Madingley Road, Cambridge CB3 0HE, United Kingdom

Freek J. M. Hoeben, Pascal Jonkheijm, Albertus P. H. J. Schenning, and E. W. Meijer
Laboratory of Macromolecular and Organic Chemistry, Eindhoven University of Technology, P.O. Box 513, 5600 MB Eindhoven, The Netherlands

Richard H. Friend and Carlos Silva[b)]
Cavendish Laboratory, University of Cambridge, Madingley Road, Cambridge CB3 0HE, United Kingdom

(Received 5 April 2005; accepted 21 June 2005; published online 31 August 2005)

We present time-resolved photoluminescence measurements on two series of oligo-*p*-phenylenevinylene (OPV) materials that are functionalized with quadruple hydrogen-bonding groups. These form supramolecular assemblies with thermotropic reversibility. The morphology of the assemblies depends on the way that the oligomers are functionalized; monofunctionalized OPVs (MOPVs) form chiral, helical stacks while bifunctionalized OPVs (BOPVs) form less organized structures. These are therefore model systems to investigate the effects of supramolecular assembly, the effects of morphology, and the dependence of oligomer length on the radiative and nonradiative rates of π-conjugated materials. The purpose of this work is to use MOPV and BOPV derivatives as model systems to study the effect of intermolecular interactions on the molecular photophysics by comparing optical properties in the dissolved phase and the supramolecular assemblies. A simple photophysical analysis allows us to extract the intrinsic radiative and nonradiative decay rates and to unravel the consequences of interchromophore coupling with unprecedented detail. We find that interchromophore coupling strongly reduces both radiative and intrinsic nonradiative rates and that the effect is more pronounced in short oligomers. © *2005 American Institute of Physics*. [DOI: 10.1063/1.1998828]

I. INTRODUCTION

Polymeric semiconductors are now finding commercial applications in display technologies based on light-emitting diodes[1] and also promise applications in photovoltaic diodes.[2] In bulk polymeric semiconductors, interchromophore coupling, where chromophores consist of π-conjugated segments within a chain, has profound effects on the optoelectronics properties.[3] An important one is to facilitate both intrinsic and extrinsic exciton quenching processes.[4,5] Intrinsic quenching is related to splitting of excitonic states; cofacial alignment of chromophores with sufficiently small separation (3–4 Å) leads to reduced oscillator strength in the lowest excited-state transition.[6] On the other hand, extrinsic processes can be enhanced by diffusion-limited quenching at either chemical (e.g., charge-transfer) or structural (e.g., internal conversion) defects.[7] These phenomena have significant effects on the photophysics even in the weak interchromophore coupling limit (when the intermolecular coupling is smaller than the exciton-phonon coupling). We are interested in developing this understanding in a model supramolecular system with controlled structural order compared to standard polymeric semiconductor systems (conjugated polymer films). Supramolecular chemistry is a promising approach to achieve three-dimensional control of intermolecular interactions.[8] This approach allows the design of extended complex structures built through the ordered assembly of elementary building blocks in solution prior to the casting process using secondary interactions such as hydrogen bonding and π-π interaction. These need to be strong enough to lead to spontaneous self-organization but weak enough so that the process is reversible so that the effects of intermolecular interactions can be unraveled from other morphological effects. Thus supramolecular architectures may be designed to possess the processing and optoelectronic properties of polymeric semiconductors with a tailored structure to enhance a specific property such as charge mobilities.[9–11]

Here, we investigate photophysics in two series of of oligo-*p*-phenylenevinylene (OPV) derivatives. The first group of oligomers has been monofunctionalised with a ureido-*s*-triazine group (MOPV3, MOPV4 and MOPV5 with, respectively, three, four and five phenyl rings, see Fig. 1 for the molecular structures). The second group of molecules is built with MOPV derivatives and consists of two MOPVs attached with an alkyl chain (BOPV3 and BOPV4 with, respectively, two MOPV3 and MOPV4 attached).

MOPV and BOPV form oligomer dimers by quadruple hydrogen bonding in dodecane solution.[10,12] Solvophobic

[a)]Present address: Clarendon Laboratory, University of Oxford, Parks Road, Oxford OX1 3PU, United Kingdom.
[b)]Present address: Département de Physique & Regroupement québéqois sur les matériaux de pointe, Université de Montréal, C. P. 6128, Succ. centre-ville, Montréal, Québec H3C 3J7, Canada. Electronic mail: carlos.silva@umontreal.ca

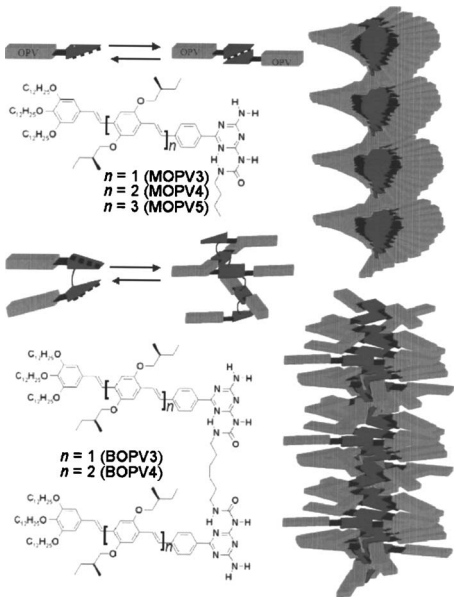

FIG. 1. Molecular structures of MOPV and BOPV derivatives and schematic representation of their packing.

and π-π interactions result in thermotropically reversible supramolecular assembly (see Fig. 1 for a schematic representation of relatively close packing of oligomers). MOPV phase transitions happen in roughly 20 °C with transition temperatures in the range 50–70 °C at the solution concentrations investigated here. Due to its dimeric structure, BOPV forms a random coil supramolecular polymer in chloroform. In dodecane, the coils collapse to frustrated stacks, bringing the OPV units closer together. By raising the temperature, the distance between the OPVs increases but the result is the stretching of the frustrated stacks and not a complete breakup, as is the case in the MOPVs. This does not result in a well-defined phase transition in BOPVs, and we observe spectral changes from roughly 40 °C to 90 °C.[13]

MOPV assemblies are chiral with a small relative angle between oligomers and a small oligomer separation. However, the alkyl linking chains in the BOPV molecules hinder the packing and lead to more disordered achiral assemblies.[10,12,14] This self-organization allows us to study excitonic processes in various morphologies of isolated supramolecular nanostructures and to compare them with excited-state phenomena in dissolved oligomer solutions.

In previous work, we explored the extrinsic consequences of intermolecular coupling, namely diffusion-assisted exciton transfer and quenching and exciton bimolecular annihilation at high exciton densities.[7,15–18] We have demonstrated that resonance energy transfer between MOPV derivatives of different length (and exciton energies) is greatly enhanced by supramolecular assembly. At low MOPV4 mole fraction ($\lesssim$2.5%), isolated MOPV4 chromophores are incorporated into MOPV3 helical assemblies as long as the solution is thermally cycled to dissolve and then re-assemble the stacks.[15,16] Optical excitation of the blended structure results in efficient energy transfer from MOPV3 hosts to MOPV4 guests, with most of the transfer occurring over the first 100 ps.

The objective of this paper is to describe the intrinsic consequences of inter-chromophore coupling by measuring radiative and nonradiative rate constants in MOPV systems, and exploring their dependence on the length of the oligomer. We find that intermolecular packing in the supramolecular structure modifies significantly the intrinsic radiative and nonradiative decay rates compared to the rates of isolated molecules. Because the supramolecular assembly process of the OPV systems described here is controlled reversibly, we can explore these issues with unprecedented detail.

II. EXPERIMENT

The synthesis of MOPV and BOPV derivatives has been described in detail elsewhere.[10,12,13] Materials were dissolved in anhydrous dodecane at concentrations around 10^{-4} M and then kept under inert atmosphere except during absorption measurements. The concentrations of the solutions were, respectively, 2.8, 1.6, 0.3, 0.7 and 0.8×10^{-4} M for MOPV3, MOPV4, MOPV5, BOPV3 and BOPV4.

We applied time-correlated single photon counting (TCSPC) to measure excited-state lifetimes and photoluminescence (PL) spectra. The solutions were excited with a pulsed diode laser [PicoQuant LDH400, 20 MHz, 70 ps full width at half-maximum (FWHM), 407 nm]. The luminescence was detected with a microchannel plate photomultiplier (Hamamatsu) coupled to a spectrometer and TCSPC electronics (Edinburgh Instruments Lifespec-ps and VTC900 PCI card). The temporal resolution is close to 80 ps, while the spectral resolution is around 4 nm. The absorption spectra were measured using a UV-visible spectrophotometer (Varian, Carry 300) with a spectral resolution lower than 1 nm.

The PL efficiencies of dilute solutions (optical density smaller than 0.1) were measured using a luminescence spectrophotometer Perkin Elmer LS50B. The excitation source was a 20 kW xenon discharge lamp (50 Hz, 8 μs FWHM, 420 nm). The PL intensities were compared to the previously measured efficiencies for a methyl end-capped OPV4 (Φ =0.76 in chloroform, see Janssen *et al.*[20]). The PL efficiencies of more concentrated solutions were obtained by comparing the PL signal of the sample in diluted and aggregated phase (see below for a discussion).

III. RESULTS

The first series of materials investigated here is oligo-*p*-phenylenevinylene derivatives consisting of three, four, and five phenyl rings in the main core (respectively called MOPV3, MOPV4, and MOPV5), monofunctionalized with a ureido-*s*-triazine end-capping group. The second series of materials is built from pairs of MOPV3 and MOPV4 linked by an alkyl chain in the functional end-capping group (respectively called BOPV3 and BOPV4). In solution, all these materials form dimers by quadruple hydrogen bonding. In apolar solvents and below a transition temperature[12,13] the dimers self-assemble into the supramolecular architectures depicted in Fig. 1. The absorption and photoluminescence (PL) spectra of MOPV derivatives at 14 °C and 90 °C are shown in Fig. 2. The excitation laser used to measure the PL had an emission wavelength of 407 nm, above (for MOPV5,

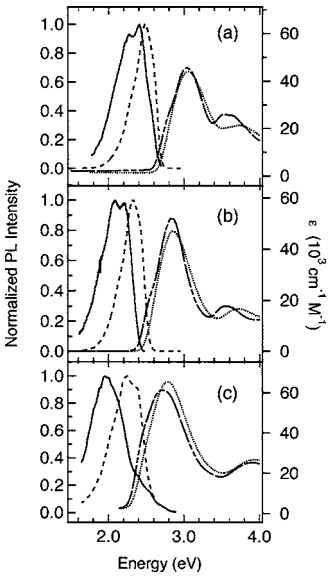

FIG. 2. Absorbance and PL spectra of MOPV3 (a), MOPV4 (b) and MOPV5 (c). The left axis is the normalized PL intensities in the dissolved (90 °C, dashed lines) and aggregated phases (14 °C, continuous lines). The right axis is the decadic molar extinction coefficient in the dissolved (90 °C, dotted lines) and aggregated phases (14 °C, long-dash lines).

MOPV4) or just below (for MOPV3) the peak of the (π,π^*) band. A red shift of the PL (in the order of 0.2 eV) and the appearance of a new absorption shoulder in the red edge of the main band are observed upon cooling the solutions and have been previously attributed to the formation of supramolecular assemblies and interchromophore coupling.[7,10] The photoluminescence spectra of BOPV derivatives are shown in Fig. 3 together with their room temperature absorption spectrum. As for MOPV derivatives, the excitation laser wavelength (407 nm) was just above the peak of the (π,π^*) band. We observe a red shift of the PL upon cooling the solutions (in the order of 0.2 eV for BOPV4 but smaller for BOPV3) and a red shoulder in the absorption spectra. By analogy with MOPV derivatives, they have been attributed to the formation of supramolecular assemblies and interchromophore coupling. We used the same experimental conditions as previous studies (temperature around 14 °C and concentrations between 10^{-5} M and 10^{-4} M) which investigated these supramolecular stacks.[7,15–18] Small-angle neutron scattering experiments showed cylindrical architectures with average stack lengths of 150 nm and radius 3 nm for MOPV4, and 60 nm and radius 2.5 nm for MOPV3. For MOPV derivatives, the cylinders consist of stacked dimers in a helical fashion based on the observed circular dichroism. The exact configuration of the stacked dimers is not known precisely but other experiments point toward small oligomer separation and small relative angle.[10,12,15] For BOPV derivatives, the absence of any circular dichroism points toward achiral stacks. As the alkyl chains hinder the packing, the BOPV dimers are stacked with random oligomer relative angle.[10]

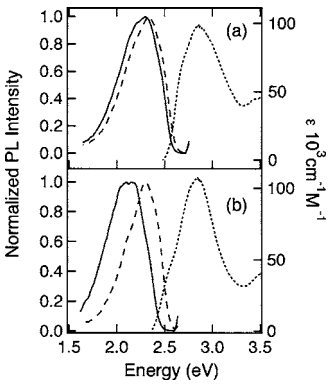

FIG. 3. Absorbance and PL spectra of BOPV3 (a) and BOPV4 (b). The left axis is the normalized PL intensities in the dissolved (90 °C, dashed lines) and aggregated phases (14 °C, continuous lines). The right axis is the decadic molar extinction coefficient in the aggregated phases (25 °C, dotted lines).

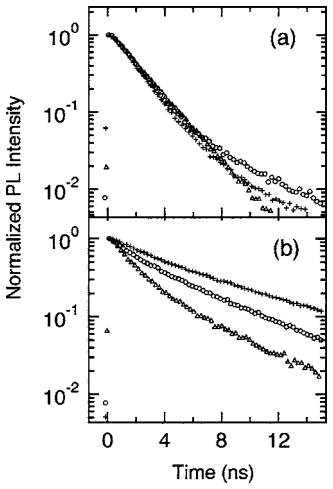

FIG. 4. Spectrally integrated PL decay of MOPV3 (crosses), MOPV4 (open circles) and MOPV5 (open triangles) at 90 °C (a) in the dissolved phase and 14 °C (b) in the aggregated phase.

Above a certain transition temperature, which depends on the material and the concentration (between 45 °C and 75 °C for MOPV derivatives) the thermodynamic equilibrium shifts from supramolecular assembly to a dissolved phase.[10] For MOPV derivatives, within a relatively narrow range (~20 °C) about the transition temperature, the positional disorder in the stacks increases and the average assembly length decreases. However, for BOPV derivatives the transition is more gradual (approximately from 30 °C to 90 °C, see Ref. 13). For the MOPV derivatives and for BOPV4, the PL spectra show that at 90 °C the red shoulders have already decreased significantly suggesting that the intermolecular coupling is much smaller at 90 °C. Therefore, we can use these two experimental conditions (14 °C and 90 °C) to compare exciton dynamics with and without strong intermolecular coupling. For BOPV3, the change in the PL spectrum is not as dramatic as for BOPV4. This is probably because the stacks are not dissolved to the same extent. However, we can use the low temperature data (14 °C) to study the exciton dynamics in the supramolecular assembly.

The PL decay of the MOPV derivatives at 14 °C and 90 °C are shown in Fig. 4. The decay curves are roughly exponential, apart from a fast initial decay (until $\approx$1 ns)[7] and a small tail at very long times after excitation (>8 ns). For the three MOPV derivatives, aggregation leads to an increase in excitonic lifetime. The lifetimes are very similar for the

TABLE I. Photophysical parameters of MOPV derivatives. MOPV3, MOPV4, and MOPV5 correspond to $n=1$, 2, and 3, respectively.

n	T (°C)	τ (ns)	Φ	x	k_r (s^{-1})	k_{nr} (s^{-1})
1	90	1.9	0.82	—	$(4.4\pm0.6)\times10^8$	$(1.0\pm0.2)\times10^8$
2	90	1.9	0.63	—	$(3.3\pm0.5)\times10^8$	$(1.9\pm0.3)\times10^8$
3	90	2.0	0.29	—	$(1.4\pm0.2)\times10^8$	$(3.4\pm0.5)\times10^8$
1	14	6.8	0.25	2.3±0.7	$(1.2\pm0.5)\times10^8$	$(0.3\pm0.5)\times10^8$
2	14	4.9	0.18	0.9±0.4	$(0.7\pm0.3)\times10^8$	$(1.3\pm0.3)\times10^8$
3	14	3.8	0.10	0.9±0.4	$(0.5\pm0.3)\times10^8$	$(2.1\pm0.3)\times10^8$

three MOPV derivatives in the dissolved phase but significantly different in the aggregated phase (see Table I). The similarities in exciton lifetimes of MOPV derivatives at 90 °C are another indication that our experimental temperature is sufficient to dissolve effectively all the stacks and measure the properties of isolated molecules (similar lifetimes independent of oligomer length were obtained for a related series of oligomers).[4] The differences in exciton lifetimes of MOPV derivatives at 14 °C can be explained in various ways, such as differences in stack configuration leading to variations in the magnitude of the intermolecular electronic coupling or the existence of nonemissive trap states with different densities in the three materials.

The PL decay of the BOPV derivatives at 14 °C and 90 °C are shown in Fig. 5. Contrary to the MOPV decays, the BOPV decays are nonexponential at all temperatures. The decays are slightly slower at 14 °C but a simple lifetime cannot be extracted. In a previous publication describing femtosecond-resolved transient PL measurements in MOPV4,[7] we showed that a stretched exponential function of the form $a\exp(bt^c)$ describes the PL decay of the supramolecular assemblies from picosecond timescales until roughly 1 ns. We identified this time-dependent decay mechanism as diffusion to dark trap sites and invoked models relating c to the lattice dimensionality d by $c=d/(d+2)$. We argued that multistep exciton diffusion on a quasi-one-dimensional lattice is a plausible description of exciton dynamics in MOPV over short timescale because nearest-neighbor interactions are expected to play a dominant role. At longer times, excitons become trapped in local minima of the potential energy landscape and need to interact with suitable transfer sites that are located further away. This leads to higher lattice dimensionality and reduces the effective diffusion coefficient. As the exciton energy decreases, this time-dependent decay channel disappears gradually.[7] For our present study, we also fitted the BOPV decays with stretched exponentials to extract the time exponents (c). At 14 °C (in the aggregated phase), c is close to 0.6 (respectively, 0.71 and 0.72 for BOPV3 and BOPV4); at 90 °C (in the more dissolved phase), c is closer to 1 (respectively, 0.83 and 1.0 for BOPV3 and BOPV4). This is a strong indication that for BOPV derivatives, the diffusion to quenching sites is still significant on nanosecond timescales and leads to nonexponential decay (contrary to what was found for MOPV derivatives). The time exponent $c\approx0.6$ at 14 °C (in the aggregated phase) is characteristic of a three-dimensional diffusion [$c=d/(d+2)$ where d is the dimension of the lattice]. Note that the time exponent c can be held to 0.6 without decreasing the fit quality significantly but it cannot be held to 0.5 (two dimensions) or 0.33 (one dimensions). At 90 °C, the time exponent is closer to 1 as expected in the absence of supramolecular assembly and diffusion mechanism. The smaller value of c for BOPV3 is another indication that the stacks are not completely dissolved. The results from the fitting procedure are given in Table II.

For MOPV derivatives, the PL efficiencies were measured in the dissolved phase (in dodecane solution at concentrations smaller than 10^{-5} M, with an optical density smaller than 0.1 and at room temperature) using standard techniques outlined in Sec. II. We assume that these are independent of temperature and concentration as long as the molecules are in the dissolved phase. From the PL efficiencies in the dissolved phase, those in the aggregated phase were inferred by comparing the total PL intensity detected divided by the number of photons absorbed in the two phases (in dodecane at concentrations $\sim10^{-4}$ M and at 14 °C and 90 °C). This factor is proportional to the PL efficiency if self-absorption can be neglected. As the absorption spectra do not change dramatically between the two phases, we neglect the change in self-absorption and use the PL intensities of the solutions in the two phases to obtain the PL efficiencies in the aggregated phase.

Radiative and nonradiative decay rate constants can be obtained from the PL efficiencies and lifetimes. As the duration of the excitation pulses used for PL efficiency measurements (8 μs) is much longer than the exciton lifetime (a few ns), the experimental conditions are close to continuous-wave excitation (CW). During the measurements, excitons

TABLE II. Fit parameters of BOPV derivatives. BOPV3 and BOPV4 correspond to $n=1$ and 2, respectively.

n	T (°C)	b (ns^{-c})	c (free)	b (ns^{-c})	c (fixed)
1	90	0.56±0.01	0.83±0.01	0.42±0.01	1.0
2	90	0.50±0.01	1.0±0.01	0.52±0.01	1.0
1	14	0.69±0.01	0.71±0.01	0.88±0.01	0.6
2	14	0.64±0.01	0.72±0.01	0.81±0.01	0.6

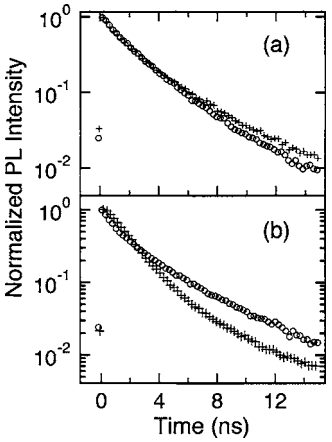

FIG. 5. Spectrally integrated PL decay of BOPV3 (a) and BOPV4 (b) at 90 °C (crosses) in the dissolved phase and 14 °C (open circles) in the aggregated phase.

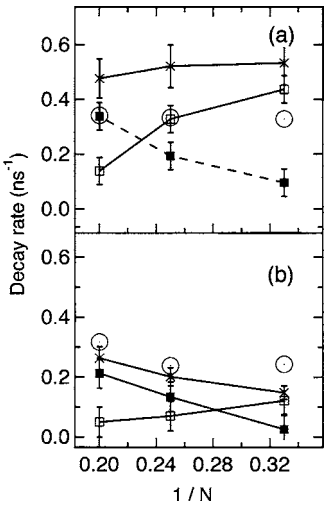

FIG. 6. Exciton decay rate constants for MOPV derivatives plotted against the inverse number of phenyl rings at 90 °C (a) in the dissolved phase and 14 °C (b) in the aggregated phase. Total decay rate constant (crosses), radiative decay rate constant (open squares), nonradiative decay rate constant (filled squares) and the radiative decay rate constant predicted by a Strickler–Berg analysis (open circle) are shown.

are generated in steady state and the instantaneous population is a distribution of excitons of various ages (where the age is the time elapsed since the creation of the exciton). Excitons can diffuse to dark trap sites in the first few hundred picoseconds[7] but, for MOPV derivatives, this decay channel disappears gradually as the exciton diffusion coefficient decreases when the exciton energy decreases.[7,16] After one exciton lifetime, the surviving exciton population can be treated as fixed. As our exciton lifetime measurements are made on nanosecond timescales, they exclude this nonradiative decay channel. Using previous data from PL up-conversion measurements,[7] we can estimate the proportion of excitons that decay by diffusion-assisted quenching. To do this, we combine the up-conversion and the TCSPC data (spectrally integrated and corrected for the effects of polarization anisotropy) to obtain a plot of the PL intensity from 1 to 50 ps. Then, we fit it with an exponential decay using the lifetime from the TCSPC data measured on nanosecond timescales. The initial amplitude of the exponential fit (A) is smaller than the initial amplitude of the data (normalized to 1) as the fit cannot reproduce this fast additional decay channel. In the following, we will label the fast additional decay channel as extrinsic diffusion to trap sites and consider that the long-time decay channels are intrinsic time-independent channels. The intrinsic channels might be time-dependent at very early times (before exciton relaxation for instance) but this does not matter for the study of exciton decay rates on nanosecond timescales.

From A, we evaluate x, the ratio of the number of excitons that decay through diffusion to trap sites (extrinsic mechanism) divided by the number of excitons that decay through intrinsic mechanisms:

$$x = \frac{n_x}{n_r + n_{nr}} = \frac{1 - A}{A}, \tag{1}$$

where n_i is the average number of excitons that decay through the channel i per second:

$$n_x = \int_0^\infty p(u) k_x(u) du, \tag{2}$$

$$n_r = \int_0^\infty p(u) k_r \, du = k_r, \tag{3}$$

$$n_{nr} = \int_0^\infty p(u) k_{nr} \, du = k_{nr}, \tag{4}$$

where $p(u)$ is the probability to find an exciton with the age u, $k_x(u)$ is the extrinsic decay rate constant of excitons of age u through diffusion to traps, k_r is the intrinsic radiative decay rate constant of excitons (assumed to be independent of the exciton age) and k_{nr} is the intrinsic nonradiative decay rate constant of excitons (assumed to be independent of the exciton age). The CW PL efficiency is

$$\Phi = \frac{n_r}{n_r + n_{nr} + n_x}. \tag{5}$$

The exciton lifetime measured on nanosecond timescales is

$$\tau = \frac{1}{k_r + k_{nr}}. \tag{6}$$

With these notations, we obtain

$$k_r = \frac{\Phi}{\tau}(1 + x), \tag{7}$$

$$k_{nr} = \frac{1 - \Phi(1 + x)}{\tau}. \tag{8}$$

The estimates of the ratio x, the lifetime τ, the efficiency Φ and the decay rate constant k_i are shown in Table I. The decay rates are also plotted against the inverse oligomer length in Fig. 6. To estimate x, we used PL up-conversion data for MOPV3 and MOPV4 solutions as described above (see Herz *et al.*[7] and Hoeben *et al.*[15]). For MOPV5, unpublished data from femtosecond transient absorption experiments[19] show that on ultrafast timescales, the PL decay

TABLE III. Results of a Strickler–Berg analysis for MOPV derivatives. MOPV3, MOPV4, and MOPV5 correspond to $n=1$, 2, and 3, respectively.

n	T (°C)	k_r (s^{-1})	Oscillator strength	k_r^{SB} (s^{-1})
1	90	$(4.4\pm0.6)\times10^8$	0.67	3.3×10^8
2	90	$(3.3\pm0.5)\times10^8$	0.78	3.3×10^8
3	90	$(1.4\pm0.2)\times10^8$	1.14	3.4×10^8
1	14	$(1.2\pm0.5)\times10^8$	0.60	2.4×10^8
2	14	$(0.7\pm0.3)\times10^8$	0.72	2.4×10^8
3	14	$(0.5\pm0.3)\times10^8$	1.13	3.1×10^8

of MOPV5 is very similar to that of MOPV4, therefore we approximate the x value of MOPV5 to that of MOPV4. The intrinsic decay rates obtained are estimates that depend on the PL efficiencies and on the ratio x. This ratio is an approximation as we are limited to a resolution of several hundred femtoseconds and cannot take into account ultrafast phenomena that would decrease the initial exciton population. However, with this method, we have access to estimates of intrinsic decay rates that were not available using the PL efficiencies alone. The results show a clear decrease of radiative decay rate and increase of nonradiative decay rate with the oligomer length. The latter was also observed with a series of similar oligomers together with a small increase in the radiative decay rate.[20] The decrease in radiative decay rate constant with increasing oligomer length observed here is related to the dramatic decrease in the PL efficiency in this series of materials. We note that this trend is more significant than what could be explained by experimental errors. The only factor that could increase the radiative decay rate constant is a time-dependent nonradiative decay channel but this is quantified in our analysis using PL decay measurements on ultrafast timescales.

IV. DISCUSSION

To understand the trend in radiative decay rate constants obtained for MOPV derivatives, and the importance of intermolecular electronic coupling, we estimated the expected radiative decay rate constants from the Strickler and Berg formalism.[21–23] This formula is related to the Einstein coefficients for absorption and spontaneous emission and is valid for strongly allowed transitions if the molecular relaxation in the excited state is small:

$$k_r = \frac{8\pi 0.2303 n^2}{c^2 N_A}\left(\int \frac{f(\bar{\nu})}{\bar{\nu}^3} d\bar{\nu}\right)^{-1} \int \frac{\epsilon(\bar{\nu})}{\bar{\nu}} d\bar{\nu}, \tag{9}$$

where n is the refractive index, N_A the Avogadro constant, c the speed of light in vacuum, $f(\bar{\nu})$ the PL spectrum normalized to unit intensity in a wavenumber energy scale, and $\epsilon(\bar{\nu})$ is the decadic molar extinction coefficient spectrum (in units of $cm^{-1}\,M^{-1}$). The integrals are over the PL and π-π^* absorption bands.

We evaluated Eq. (9) for the three MOPV derivatives both in dissolved and in aggregated phases using the time-integrated experimental spectra. The results are shown in Table III and plotted in Fig. 6 as large open circles. The predicted decay rate for MOPV4 in the dissolved phase is very close to the experimental one. However, the predicted values for MOPV3 and MOPV5 in the dissolved phase are slightly different as the model cannot reproduce the experimental trend of decrease in radiative decay rate when the oligomer length increases. Note that a similar increase in predicted radiative decay rates was also found with similar oligomers.[20] In the Strickler–Berg formalism, the increase in oscillator strength is compensated by the decrease in average PL frequency. The difference between predicted and experimental radiative decay rate constants could be related to the breakdown of the Strickler and Berg model.[22] The discrepancies could also be linked to some residual interchromophore couplings as some stacks are not completely dissolved (the long-lived tails in the PL decays of MOPV derivatives points toward such an explanation).

The predicted decay rates for MOPV derivatives in the aggregated phase are too high by more than a factor of 2. These large discrepancies are related to the interchromophore coupling. In a cofacial dimer, these couplings lead to excitonic splitting with the oscillator strength concentrated in the upper excited state[6] while the exciton will very quickly relax to the lower one. In our system, a similar situation is plausible with a very small relative angle between neighboring oligomers. This does not change dramatically the oscillator strength of the absorption but decreases significantly the radiative decay rates with respect to the isolated molecules. The breakdown of the Strickler–Berg formula is an indication here of the interchromophore coupling. To predict the radiative decay rates, a much more complex analysis is needed to calculate the exact wavefunctions and matrix elements. This would need to take into account configurational relaxation of the excited state and interchromophore coupling in the aggregated phase.

The intrinsic nonradiative decay rate constants increase significantly with the oligomer length both in dissolved and in aggregated phases (this reproduces the results obtained for similar molecules[20]). This increase cannot be explained by a decrease in relaxation energy and excited-state distortion alone as the decrease in the Stokes shift with increase in conjugation length is very modest (the Stokes shifts are, respectively, 0.4, 0.38, and 0.35 eV for MOPV3, MOPV4, and MOPV5 and do not change significantly upon aggregation; see Fig. 2). A different approach is to relate the nonradiative decay rates to the number of phonons needed to dissipate the energy. We consider an energy-gap law often used to describe such phonon emission:[24,25]

$$k_{nr} \propto \exp\left(-\gamma \frac{\Delta E}{\hbar\omega}\right), \tag{10}$$

where ΔE is the energy difference between the excited-state and the ground-state, $\hbar\omega$ is the effective phonon energy and γ is a characteristic electron-phonon coupling factor.[25] The energy to be dissipated in phonons corresponds to the energy of the first vibronic peak of the PL spectra (E_0). To estimate those energies, we fitted the PL spectra with a sum of Gaussians of constant width (σ) and regular spacing (Δ):

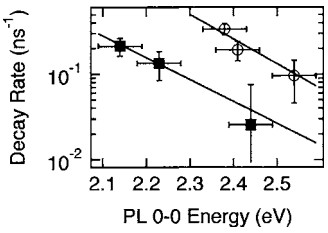

FIG. 7. Intrinsic nonradiative decay rate constants for MOPV derivatives plotted against the energy of the first vibronic peak of the PL spectra at 90 °C (open circles) in the dissolved phase and 14 °C (filled squares) in the aggregated phase. The lines are fits to the energy gap law [Eq. (10)] with $\gamma=1$.

$$I=\sum_{j=1}^{N} A_j \exp\left(-\frac{(E-E_0-j\Delta)^2}{2\sigma^2}\right). \tag{11}$$

The plot of nonradiative decay rate constants against the energy of the first vibronic peak of the PL spectra is shown in Fig. 7. The data can be fitted with an exponential law which validates qualitatively our procedure. If we estimate $\hbar\omega$ to be the spacing of the vibronic progression (Δ) which does not vary significantly with the oligomer length ($\Delta\approx 0.15$ eV in the dissolved phase and $\Delta\approx 0.17$ eV in the aggregated phase), then the factor γ is close to one for both the dissolved phase and the aggregated phase:

$$k_{nr}\propto \exp\left(-\frac{E_{PL}^{0-0}}{\hbar\omega}\right). \tag{12}$$

From the PL spectra, we know that the spacing between the vibronic peaks and their amplitudes changes upon aggregation. Our data show qualitatively that the couplings of the vibronic modes change upon aggregation significantly enough to decrease the nonradiative decay rates but these changes are modest enough for the energy-gap law coefficient to remain constant upon aggregation.

V. CONCLUSION

We have explored the photophysical consequences of supramolecular assembly of oligo-*p*-phenylenevinylene derivatives in dilute solution. The main conclusion of this work is that a complete description of photophysics of organic semiconductors needs to include the effect of close packing on both intrinsic and extrinsic properties.

We have shown that the packing of MOPV derivatives modifies the intrinsic radiative and nonradiative decay rate constants. This was possible using time-resolved photoluminescence spectroscopy to estimate the intrinsic and extrinsic nonradiative decay rate constants. We find that the radiative decay rate constants are significantly reduced with the splitting of the excited states induced by the molecular packing. The origin of the reduction in the nonradiative decay rate is less evident. The effects of interchromophore couplings are more important for short oligomers.

MOPV and BOPV derivatives represent a very good model system to study these effects as they possess polymeric optoelectronic properties in the aggregated phase but with the additional tunability and structural control afforded by supramolecular chemistry.

ACKNOWLEDGMENTS

The work in Cambridge was supported by the UK Engineering and Physical Sciences Research Council (EPSRC) and the EPSRC-funded interdisciplinary research center for nanotechnology (Cambridge, UCL, Bristol). C.D. was an Isaac Newton Scholar. C.S. was an EPSRC Advanced Research Fellow. The Work in Eindhoven is supported by the Netherlands Organization for Scientific Research (NWO, CW). The Cambridge-Eindhoven collaboration was supported by the European Commission (LAMINATE).

[1] R. H. Friend, R. W. Gymer, A. B. Holmes, J. H. Burroughes, R. N. Marks, C. Taliani, D. D. C. Bradley, D. A. DosSantos, J. L. Brédas, M. Lögdlund, and W. R. Salaneck, Nature (London) **397**, 121 (1999).
[2] C. J. Brabec, C. Winder, N. S. Sariciftci, J. C. Hummelen, A. Dhanabalan, and P. A. van Hal, R. A. J. Janssen, Adv. Funct. Mater. **12**, 709 (2002).
[3] See B. J. Schwartz, Annu. Rev. Phys. Chem. **54**, 141 (2003), and references therein.
[4] C. M. Heller, I. H. Campbell, B. K. Laurich, D. L. Smith, D. D. Bradley, P. L. Burn, J. P. Ferraris, and K. Müllen, Phys. Rev. B **54**, 5516 (1996).
[5] D. Beljonne, G. Pourtois, C. Silva, E. Hennebicq, L. M. Herz, R. H. Friend, G. D. Scholes, S. Setayesh, K. Müllen, and J. L. Brédas, Proc. Natl. Acad. Sci. U.S.A. **99**, 10982 (2002).
[6] J. Cornil, D. A. dos Santos, X. Crispin, R. Silbey, and J. L. Brédas, J. Am. Chem. Soc. **120**, 1289 (1998).
[7] L. M. Herz, C. Daniel, C. Silva, F. J. M. Hoeben, A. P. H. J. Schenning, E. W. Meijer, R. H. Friend, and R. T. Phillips, Phys. Rev. B **68**, 045203 (2003).
[8] J. M. Lehn, *Supramolecular Chemistry* (VCH, Weinheim, 1995).
[9] A. M. van de Craats, J. M. Warman, A. Fechtenkötter, J. D. Brand, M. A. Harbison, and K. Müllen, Adv. Mater. (Weinheim, Ger.) **11**, 1469 (1999).
[10] A. P. H. J. Schenning, P. Jonkheijm, E. Peeters, and E. W. Meijer, J. Am. Chem. Soc. **123**, 409 (2001).
[11] V. Percec, M. Glodde, T. K. Bera, Y. Miura, I. Shiyanovskaya, K. D. Singer, V. S. K. Balagurusamy, P. A. Heiney, I. Schnell, A. Rapp, H.-W. Spiess, S. D. Hudsonk, and H. Duank, Nature (London) **419**, 384 (2002).
[12] P. Jonkheijm, F. J. M. Hoeben, R. Kleppinger, J. van Herrikhuyzen, A. P. H. J. Schenning, and E. W. Meijer, J. Am. Chem. Soc. **125**, 15941 (2003).
[13] F. J. M. Hoeben, A. P. H. J. Schenning, and E. W. Meijer, ChemPhysChem (to be published).
[14] P. Jonkheijm, J. K. J. van Duren, P. T. Herwig, K. T. Hoekerd, R. A. J. Janssen, M. Kemerink, E. W. Meijer, A. P. H. J. Schenning, and H. F. M. Schoo, Adv. Funct. Mater. (submitted).
[15] F. J. M. Hoeben, L. M. Herz, C. Daniel, P. Jonkheijm, A. P. H. J. Schenning, C. Silva, S. C. J. Meskers, D. Beljonne, R. T. Phillips, R. H. Friend, and E. W. Meijer, Angew. Chem., Int. Ed. **43**, 1976 (2004).
[16] C. Daniel, L. M. Herz, C. Silva, F. J. M. Hoeben, A. P. H. J. Schenning, and E. W. Meijer, Synth. Met. **147**, 29 (2004).
[17] C. Daniel, L. M. Herz, C. Silva, F. J. M. Hoeben, A. P. H. J. Schenning, and E. W. Meijer, Phys. Rev. B **68**, 235212 (2003).
[18] A. P. H. J. Schenning, P. Jonkheijm, F. J. M. Hoeben, J. v. Herrikhuyzen, S. C. J. Meskers, E. W. Meijer, L. M. Herz, C. Daniel, C. Silva, R. T. Phillips, R. H. Friend, D. Beljonne, A. Miura, S. De Feyter, M. Zdanowska, H. Uji-i, F. C. De Schryver, Z. Chen, F. Würthner, M. Mas-Torrent, D. den Boer, M. Durkut, and P. Hadley, Synth. Met. **147**, 43 (2004).
[19] C. Daniel, Ph.D. thesis, University of Cambridge (2004).
[20] E. Peeters, A. M. Ramos, S. C. J. Meskers, and R. A. J. Janssen, J. Chem. Phys. **112**, 9445 (2000).
[21] J. N. Murell and J. A. Pople, Proc. Phys. Soc. London **A69**, 245 (1956).
[22] S. J. Strickler and R. A. Berg, J. Chem. Phys. **37**, 814 (1962).
[23] J. R. Bolton and M. D. Archer, J. Phys. Chem. **95**, 8453 (1991).
[24] D. Polli, G. Cerullo, G. Lanzani, S. De Silvestri, H. Hashimoto, and R. J. Cogdell, Synth. Met. **139**, 893 (2003).
[25] M. Pope and C. E. Swenberg, *Electronic Processes in Organic Crystals and Polymers* (Oxford University Press, Oxford 1982).